

Turbulent transport of alpha particles in tokamak plasmas

A. Croitoru,^{1,2,*} D. I. Palade,^{1,2} M. Vlad,¹ and F. Spineanu¹

¹*National Institute of Laser, Plasma and Radiation Physics,
PO Box MG 36, RO-077125 Măgurele, Bucharest, Romania*

²*Faculty of Physics, University of Bucharest, Romania*

We investigate the $\mathbf{E} \times \mathbf{B}$ diffusion of fusion born α particles in tokamak plasmas. We determine the transport regimes for a realistic model that has the characteristics of the ion temperature gradient (ITG) or of the trapped electron modes (TEM) driven turbulence. It includes a spectrum of potential fluctuations that is modeled using the results of the numerical simulations, the drift of the potential with the effective diamagnetic velocity and the parallel motion. Our semi-analytical statistical approach is based on the decorrelation trajectory method (DTM), which is adapted to the gyrokinetic approximation. We obtain the transport coefficients as a function of the parameters of the turbulence and of the energy of the α particle. According to our results, significant turbulent transport of the α particles can appear only at energies of the order of 100KeV. We determine the corresponding conditions.

* c.m.andreea@gmail.com

I. INTRODUCTION

The turbulent transport of the fast α particles was considered negligible in tokamak plasmas [1] due to the fast gyration motion with a Larmor radius much larger than the correlation length, which leads to a very small amplitude of the gyro-average potential. However, this problem was reconsidered in the last decade [2–14], in preparation of the Tritium experiments in JET and ITER. The conclusions are rather dispersed, from completely negligible turbulent transport [15] to diffusion coefficients that can be larger than those of plasma ions [16, 17].

Most of the theoretical studies of α particle turbulent transport are self-consistent numerical simulations of turbulence and α particles turbulent fluxes. Other studies use the test particle approach in numerical simulations based on constructed potentials or on the results of turbulence simulations. The characteristics of turbulence and the α particle fluxes are determined in the first case as functions of the macroscopic conditions (gradients, heating power). The second approach obtains the diffusion coefficient of the α particles as a function of their energy and of the characteristics of the turbulence. It allows to find if the turbulent loss of α particles can be significant and to identify the corresponding conditions.

This paper is included in the last category. We determine the transport regimes of the α particles as a function of their energy for a realistic model of turbulence. The spectrum of the stochastic potential has the shape of the ion temperature gradient (ITG) or of the trapped electron modes (TEM) driven turbulence. The drift of the potential with the effective diamagnetic velocity and the parallel motion of the fast particles are included in the model. The main result consists in the evaluation of the energy corresponding to the maximum turbulent transport D_{\max} . We show that D_{\max} does not always appear when the α particles reach the energy of the plasma ions (for the ashes), but it can correspond to larger energies.

We use a semi-analytical approach based on the decorrelation trajectory method (DTM) [18, 19] in the gyrokinetic approximation developed in [7].

The article is organized as follows. Section II contains the basic equations and the statistical approach based on the DTM for the Lorentz transport in the gyro-kinetic approximation for a Maxwellian distribution of Larmor radii. In section III we present the transport regimes for different ranges of the parameters and obtain the energy dependence of the α particles diffusion coefficient. The conclusions are summarized in section IV.

II. MODEL AND STATISTICAL METHOD

A. Equations of motion for fast ions

The turbulent transport of the fast ions is studied in the test particle approach starting from the Newton-Lorentz equations of motion in a stochastic potential $\phi(x_1, x_2, z, t)$ and a constant magnetic field $\mathbf{B} = B\mathbf{e}_z$ oriented along the z axis

$$\begin{aligned}\frac{du_i(t)}{dt} &= -\frac{q}{m_\alpha} \frac{\partial \phi(x_1, x_2, z, t)}{\partial x_i} + \Omega_\alpha \varepsilon_{ij} u_j, \\ \frac{dx_i(t)}{dt} &= u_i, \\ \frac{dz(t)}{dt} &= u_z.\end{aligned}\tag{1}$$

Where $\mathbf{x}(t) = (x_1(t), x_2(t))$ is the ion displacement in the plane perpendicular to \mathbf{B} , $u_i, i = 1, 2$ are the components of the velocity in this perpendicular plane, u_z is the velocity along the magnetic field, m_α is the ion mass, q is its charge, $\Omega_\alpha = qB/m_\alpha$ is the cyclotron frequency and ε_{ij} is the antisymmetric tensor ($\varepsilon_{12} = 1$, $\varepsilon_{21} = -1$, $\varepsilon_{ii} = 0$).

The potential $\phi(x_1, x_2, z, t)$ is modeled as a stationary and homogeneous Gaussian stochastic function. Its spectrum $S(k_1, k_2, z, t)$ corresponds to the general characteristics of the ITG or TEM turbulence. Since the spectrum at saturation is mainly determined by the ion dynamics, its shape is similar for both types of turbulence. The only difference is given by the value of the typical wave numbers ($k_2 \rho_{ion} \lesssim 1$ for ITG, $k_2 \rho_{ion} \approx 1$ for TEM). The spectrum has two symmetrical maxima for $k_2 = \pm k_0$, $k_1 = 0$, and zero amplitude for $k_2 = 0$. We use the simple analytical expression of $S(\mathbf{k})$ that was found in [20] to be in agreement with numerical and experimental results of [21, 22]

$$S(k_1, k_2, z, t) \propto \Phi^2 \exp\left(-\frac{|z|}{\lambda_z} - \frac{|t|}{\tau_c}\right) \frac{k_2}{k_0} \exp\left(-\frac{k_1^2}{2} \lambda_1^2\right) \left[\exp\left(-\frac{(k_2 - k_0)^2}{2} \lambda_2^2\right) - \exp\left(-\frac{(k_2 + k_0)^2}{2} \lambda_2^2\right) \right]. \quad (2)$$

The parameters of this function are the amplitude of the potential fluctuations Φ , the correlation lengths along each direction λ_i , $i = 1$ (radial), $i = 2$ (poloidal), $i = z$ (parallel), and the correlation time τ_c . The Fourier transform of $S(k_1, k_2, z, t)$ is the Eulerian correlation (EC) of the potential.

The change of coordinates $(\mathbf{x}, \mathbf{u}) \longrightarrow (\boldsymbol{\xi}, E, \mu, \zeta)$ leads to

$$\frac{d\xi_i}{dt} = -\varepsilon_{ij} \frac{1}{B} \frac{\partial \phi(\boldsymbol{\xi} + \boldsymbol{\rho}, z, t)}{\partial \xi_j}, \quad (3)$$

$$\frac{d\rho_i}{dt} = \varepsilon_{ij} \left[\frac{1}{B} \frac{\partial \phi(\boldsymbol{\xi} + \boldsymbol{\rho}, z, t)}{\partial \xi_j} + \Omega_\alpha \rho_j \right], \quad (4)$$

$$\frac{dz}{dt} = u_z, \quad (5)$$

where the time dependent Larmor radius $\boldsymbol{\rho}(t)$ is defined by $\rho_i = -\varepsilon_{ij} u_j / \Omega_\alpha$, $\boldsymbol{\xi}(t)$ is the guiding center position $\boldsymbol{\xi} = \mathbf{x} - \boldsymbol{\rho}$, E is the particle energy, $\mu = u_\perp^2 / 2B$ is the magnetic moment, and ζ is the gyrophase angle.

The very large value of the cyclotron frequency $\Omega_\alpha \gg 1$ enables a strong simplification of the equation of motion by using the gyrokinetic approximation [23, 24]. The first term in the right hand side term of Eq. (4) is negligible compared to the second one, and the solution of this equation is $\boldsymbol{\rho}(t) = \rho_0 (\sin(\zeta_0 + \Omega_\alpha t), \cos(\zeta_0 + \Omega_\alpha t))$, where $\rho_0 = u / \Omega_\alpha$ and $u = \sqrt{u_1^2 + u_2^2}$. Thus, the Larmor radius ρ_0 is constant, and the time dependence is contained in the uniform gyration motion. Moreover, the time variation of the potential is slow. Its characteristic time τ_c is very large compared to the gyration period $\theta \equiv 2\pi / \Omega$, $\tau_c \gg \theta$. Since the displacement of the guiding center during θ is small, Eq. (3) can be averaged over the cyclotron period at constant $\boldsymbol{\xi}$ and t . One obtains

$$\frac{d\xi_i}{dt} = -\varepsilon_{ij} \frac{\partial_j \psi(\boldsymbol{\xi}, z, t; \rho_0)}{\partial \xi_j}, \quad (6)$$

$$\psi(\boldsymbol{\xi}, z, t; \rho_0) = \frac{1}{B} \frac{1}{\theta} \int_t^{t+\theta} d\tau \phi(\boldsymbol{\xi}(t) + \boldsymbol{\rho}(\tau), z(t), t), \quad (7)$$

where the gyro-averaged potential ψ was normalized with B . Thus, the motion of the guiding centers of the fast ions obeys the same equation as in the limit of zero Larmor radius, but with the modified potential (7). Using the Fourier representation of the potential, $\tilde{\phi}(\mathbf{k}, z(t), t)$, and performing the time integral

$$\psi(\boldsymbol{\xi}, z, t; \rho_0) = \frac{1}{B} \int d\mathbf{k}_1 d\mathbf{k}_2 \tilde{\phi}(\mathbf{k}, z(t), t) J_0(k\rho_0) \exp[i\mathbf{k} \cdot \boldsymbol{\xi}(t)], \quad (8)$$

where the wave number $\mathbf{k} = (k_1, k_2)$ is perpendicular on \mathbf{B} , $k = \sqrt{k_1^2 + k_2^2}$ and J_0 is the Bessel function of the first kind. This shows that the gyro-average of the potential ϕ determines the multiplication of its Fourier transform with $J_0(k\rho_0)$, which corresponds to the gradual attenuation of the large wave number components of the spectrum as the Larmor radius increases.

The EC of the averaged potential $\psi(\boldsymbol{\xi}, z, t; \rho_\alpha)$ for a Maxwellian distribution of particle velocities is

$$\begin{aligned} E(\boldsymbol{\xi}, z, t; \rho_\alpha) &\equiv \langle \psi(\boldsymbol{\xi}', z', t') \psi(\boldsymbol{\xi}' + \boldsymbol{\xi}, z' + z, t' + t) \rangle \\ &= \frac{1}{B^2} \int d\mathbf{k} S(\mathbf{k}, z, t) \exp[i\mathbf{k} \cdot \boldsymbol{\xi}] \int_0^\infty dv v^2 e^{-v^2} J_0^2\left(\frac{v}{\Omega_\alpha} k\right) \\ &= \frac{1}{B^2} \int d\mathbf{k} S(\mathbf{k}, z, t) \exp(-\rho_\alpha^2 k^2) I_0(\rho_\alpha^2 k^2) \exp[i\mathbf{k} \cdot \boldsymbol{\xi}], \end{aligned} \quad (9)$$

where the velocity is given in units of the thermal velocity $v_{th} = \sqrt{T_\alpha / m_\alpha}$ of the fast particles with the temperature T_α , $\rho_\alpha = v_{th} / \Omega_\alpha$ and $I_0(x)$ the modified Bessel function of the first kind. The limit $\rho_\alpha = 0$ corresponds to the EC of

the potential ϕ . The EC (9) is represented in Figure 1 for several values of ρ_α . One can see that the amplitude of $\psi(\xi, z, t; \rho_\alpha)$ is a monotonically decreasing function of ρ_α and that the effective correlation lengths in the perpendicular plane increase with ρ_α . The general shape of the EC is not changed at large ρ_α . In particular, the positive and the negative parts compensate, and the integral over x_2 is zero for any ρ_α . This property is due to the spectrum (2), which cancels for $k_2 = 0$. We plot in Figure 2 the EC of the gyro-averaged potential ψ for $\bar{\rho} = \rho_\alpha/\lambda_2 = 1.5$, $k_0 = 1$, $a = 9$ and $\Phi = 1$.

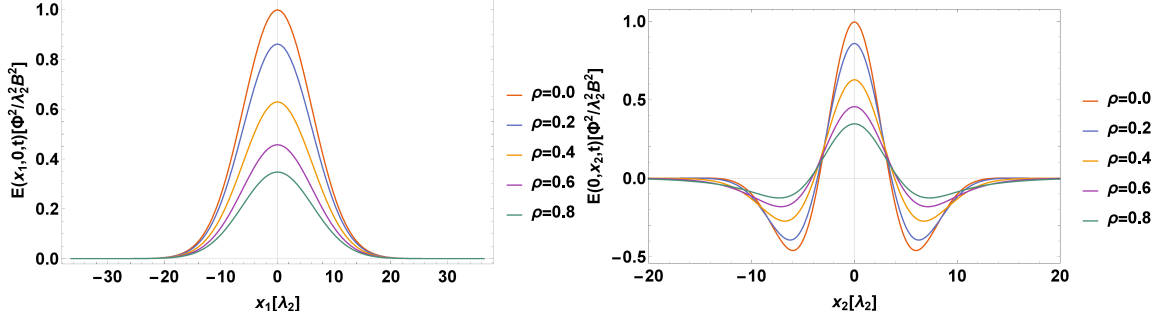


FIG. 1: The EC (9) of the averaged potential ψ for the values of the Larmor radius that label the curves.

B. The decorrelation trajectory method

The transport of fast particles in turbulent plasmas is described by equations that are similar to those for the $\mathbf{E} \times \mathbf{B}$ drift. Moreover, the shape of the EC of ψ is similar to that of ϕ . We introduce normalized quantities [25] using as units λ_2 for the perpendicular displacements, λ_z for parallel displacements, $V_0 = \Phi/B\lambda_2$ for the $\mathbf{E} \times \mathbf{B}$ drift velocity

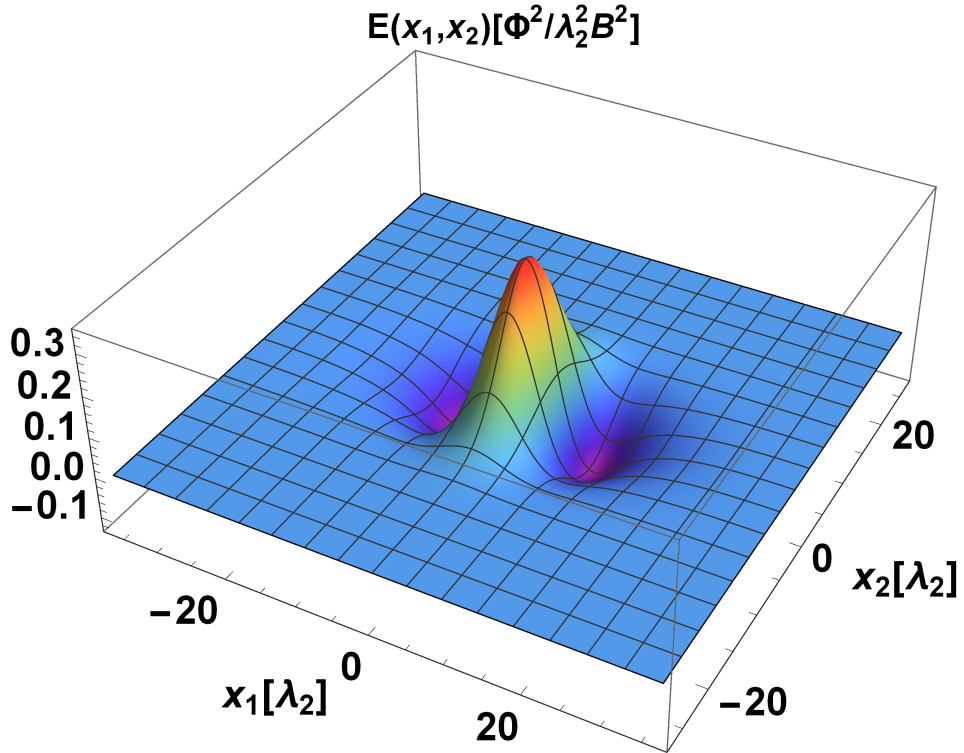


FIG. 2: $E(x_1, x_2, 0, 0; 1.5)$ for $k_0 = 1$ and $a = 9$.

and $\tau_0 = \lambda_2/V_0$ for time. The equations of motion for the normalized quantities (designed by the same symbols as the physical ones) are

$$\frac{d\xi_i}{dt} = -\varepsilon_{ij} \frac{\partial_j \psi(\boldsymbol{\xi}, z, t; \bar{\rho})}{\partial \xi_j} + \delta_{i2} V_d, \quad \frac{dz}{dt} = \frac{\tau_0}{\tau_z}, \quad (10)$$

where $\tau_z = \lambda_z/v_{th}$ is the decorrelation time induced by the parallel motion, $\bar{\rho} = \rho_\alpha/\lambda_2$, and $V_d = V_*/V_0$, with V_* being the effective diamagnetic velocity. The equation is written in a frame that moves with the potential, in which the normalized effective diamagnetic velocity appears as an average velocity.

This type of statistical problem was analyzed in several papers. The time dependent diffusion coefficients $D_i(t)$, $i = 1, 2$ were determined using the decorrelation trajectory method (DTM) [18, 19]. This is a semi-analytical method, which shows that $D_i(t)$ can be approximated using a set trajectories obtained from the EC of the potential, the decorrelation trajectories (DTs). The main idea of this method is to group together trajectories that are similar by imposing supplementary initial conditions. Each group corresponds to a subensemble S of realizations of the stochastic potential that is defined by the supplementary initial conditions. One obtains a DT for each subensemble, which then is used to evaluate $D_i(t)$ as weighted sums of the contributions of all subensembles.

We use here the fast DTM introduced in [20], which imposes only two supplementary initial conditions: the potential in the starting point of the guiding centers trajectories $\psi^0 \equiv \psi(0, 0, 0; \bar{\rho})$ and the orientation θ^0 of the normalized initial velocity. The advantage of this method is that the number of DTs is strongly reduced.

The time dependent diffusion coefficients $D_i(t)$ are obtained from

$$D_1(t) = \frac{V_1}{4} \int_{-\infty}^{\infty} d\phi^0 \exp\left(-\frac{(\phi^0)^2}{2}\right) \int_0^{2\pi} d\theta^0 \cos(\theta^0) X_1^S(t), \quad (11)$$

$$D_2(t) = \frac{V_2}{4} \int_{-\infty}^{\infty} d\phi^0 \exp\left(-\frac{(\phi^0)^2}{2}\right) \int_0^{2\pi} d\theta^0 \sin(\theta^0) X_2^S(t), \quad (12)$$

where $\mathbf{X}^S(t)$ is the DT in the subensemble S that is the solution of

$$\frac{dX_i^S}{dt} = V_i^S(\mathbf{X}^S, t) + \delta_{i2} V_d. \quad (13)$$

The subensemble average velocities $V_i^S(\mathbf{x}, t)$ are obtained from the average potential

$$\Phi^S(\mathbf{x}, t) = \phi^0 \frac{E(\mathbf{x}, t; \bar{\rho})}{E(0)} + \sqrt{\frac{8}{\pi}} \cos(\theta^0) \frac{E_2(\mathbf{x}, t; \bar{\rho})}{V_1} - \sqrt{\frac{8}{\pi}} \sin(\theta^0) \frac{E_1(\mathbf{x}, t; \bar{\rho})}{V_2}, \quad (14)$$

$$V_i^S(\mathbf{x}, t) = -\varepsilon_{ij} \frac{\partial}{\partial x_j} \Phi^S(\mathbf{x}, t), \quad (15)$$

where $E_i(\mathbf{x}, t; \bar{\rho}) \equiv \partial E(\mathbf{x}, t; \bar{\rho})/\partial x_i$ is the space derivative. An example of the subensemble potential $\Phi^S(\mathbf{x}, 0)$ is show in Figure 3. The transport at large space and time scales is described by the asymptotic value $D_i^\infty \equiv \lim_{t \rightarrow \infty} D_i(t)$.

A computer code was developed for determining $D_i(t)$ using Eqs. (11-15). It calculates the EC of ψ (9) and its derivatives that appear in the subensemble average velocity (15) using a fast Fourier Transform subroutine. The latter links an uniform grid representation in the \mathbf{k} space to a two-dimensional real space mesh on which the velocity field is computed. The spectrum (2) is used for all the calculations presented in this paper, but it can easily be replaced by other models. The DTs are determined using high order interpolation techniques for the velocity field. The time step automatically adapts so that only the space steps along x_1 and x_2 have to be optimized. The condition is provided by the trajectories with $\tau_d \rightarrow \infty$, which represent periodic motions on the contour lines of ψ . They have to remain close to these lines during the whole integration time that can be of hundreds of periods.

III. FAST PARTICLE DIFFUSION REGIMES

A. Basic physical processes

The diffusion regimes of the electrons [20] and of the ions [25] in the realistic model of the spectrum (2) were studied for the limit of zero Larmor radius. The EC of the gyro-average potential (9) contains eight physical parameters, six

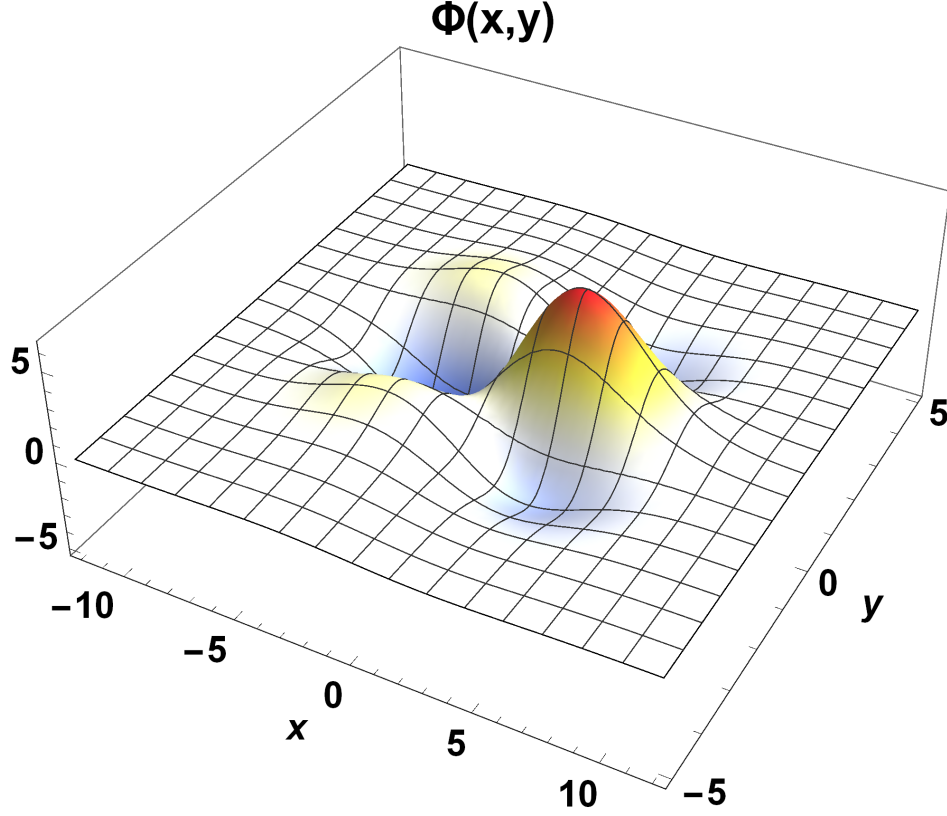


FIG. 3: The subensemble average potential $\Phi(x_1, x_2)$ defined by Eq. 14 for $\bar{\rho} = 1.5$, $k_0 = 1$, $a = 9$, $\phi^0 = 1$, $v_1^0 = 2$, $v_2^0 = 3$ and $V_d = 0$.

from the spectrum of the turbulence (2): the amplitude of the potential fluctuations, Φ , the maximum wave number k_0 , the spatial decorrelation lengths $\lambda_1, \lambda_2, \lambda_z$ and the temporal decorrelation length τ_c plus the Larmor radius, and the effective diamagnetic velocity V_* . The latter appears as the drift of the potential in the poloidal direction. We have found that the transport regimes are determined by four dimensionless parameters K_d , K_* or equivalently V_d , k_0 and a , which are defined by

$$K_d \equiv \frac{\tau_d}{\tau_0}, \quad \tau_d = \frac{\tau_c \tau_z}{\tau_c + \tau_z}, \quad (16)$$

$$K_* \equiv \frac{\tau_*}{\tau_{fly}} = \frac{V_y}{V_d}, \quad V_d = \frac{V_*}{V_0}, \quad (17)$$

$$k_0 \equiv k_0 \lambda_2, \quad (18)$$

$$a = \frac{\lambda_1^2}{\lambda_2^2}. \quad (19)$$

The values of K_d and K_* , are related to the presence of trajectory trapping or eddying in the structure of the stochastic potential.

The effective Kubo number K_d (16) is a measure of the decorrelation of the trajectories from the potential, which is determined by the time variation of the potential and/or by the parallel motion of the particles. Trajectory trapping exists when the decorrelation is weak such that the characteristic time τ_d is larger than the time of flight $\tau_{fly} = (\lambda_x/V_x + \lambda_y/V_y)$.

The diamagnetic parameter K_* (17) is a dimensionless measure of the effective velocity V_d , which determines the characteristic time $\tau_* = \lambda_y/V_d$. It is equivalent with an average potential xV_d , which adds to the stochastic potential and changes the configuration of the total potential. Bunches of opened contour lines appear on a fraction of the surface that increases from zero (for $V_d = 0$, $K_* = \infty$) to one (for $V_d > V_*$, $K_* < 1$). Trajectory trapping is possible only when the bunches of open lines fill only a fraction of the surface, and islands of closed contour lines exists between them. This configuration corresponds to the condition $V_d < V_*$, $K_* > 1$.

The main wave number k_0 (18) and the anisotropy a (19) influence the shape of the contour lines of the potential, and they only lead to changes of the parameters of the transport regimes.

The special shape of the spectrum (2) and of the EC (Figure 1) leads to similar dependences of D_1^∞ on K_d for the quasilinear regime ($K_* < 1$) and for the nonlinear regime ($K_* > 1$) [20]. In both cases, $D_1^\infty = V_1^2 \tau_d$ for small K_d , then it has a maximum at $K_d = K_{\max}$ and eventually it decays as $K_d^{-\nu}$. K_{\max} depends on the transport regime: $K_{\max} = K_* \sqrt{a}/\sqrt{k_0^2 + 3}$ for $K_* < 1$, and $K_{\max} = \sqrt{a}/\sqrt{k_0^2 + 3}$ for $K_* > 1$. The power ν also depends on the regime and on the EC of the potential. We note that, for an usual decreasing EC without negative minima, the diffusion coefficient in the quasilinear regime ($K_* < 1$) has significantly larger values at large K_d since it saturates at the maximum value instead of decaying.

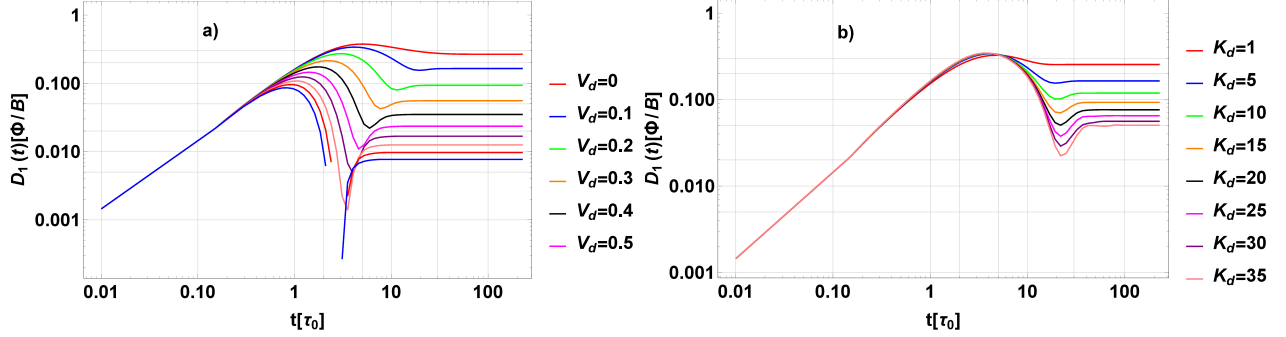


FIG. 4: a) The time dependent diffusion coefficient $D_1(t)$ for several values of V_d and b) of K_d . The other parameters are $\bar{\rho} = 4$, $k_0 = 1$ and $a = 9$

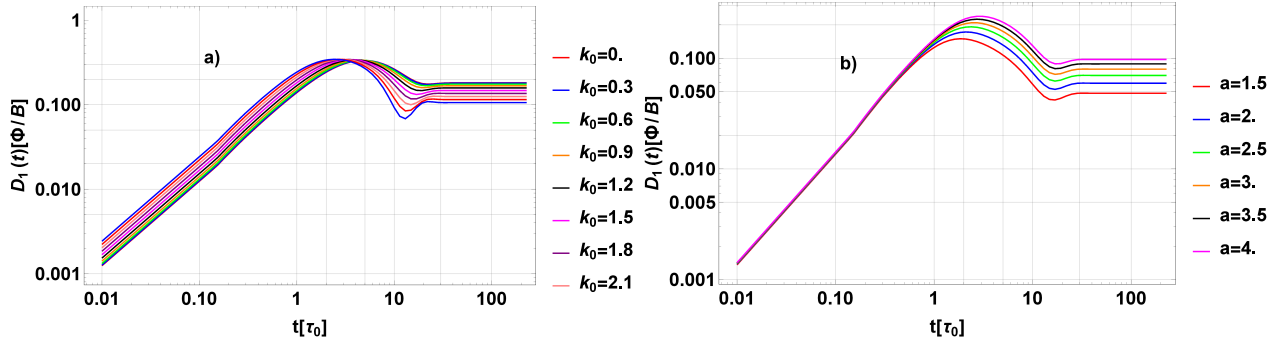


FIG. 5: a) The time dependent diffusion coefficient $D_1(t)$ for several values of k_0 and b) of a . The other parameters are $\bar{\rho} = 4$, $K_d = 10$ and $V_d = 0.1$.

The first question addressed in this paper concerns the basic physics of the transport regimes of the fast particles. We examine the dependence of the diffusion coefficient on the four parameters at a large value of the Larmor radius ($\bar{\rho} = 4$). Examples of the time dependent diffusion coefficients obtained using the DTM in the nonlinear regime are shown in Figures 4 and 5.

The effects of the decorrelation and of the average velocity in the nonlinear regime are presented in Figure 4. The decorrelation leads to the transition from the subdiffusive to diffusive transport by saturating $D_i(t)$. The process is similar with the case of small energy particles. The saturation time increases with the increase of K_d and the asymptotic diffusion coefficient decreases (Figure 4b). This is due to the fraction of non-trapped trajectories that decreases when K_d increases, leading to the decrease of D_1^∞ . The effect of the average velocity for a large value of the decorrelation parameter ($K_d = 10$) (Figure 4a) consists of the continuous decrease of the radial diffusion when \bar{V}_d increases.

The effect of the dominant wave number k_0 is shown in Figure 5a. The increase of k_0 determines the decrease of the radial diffusion coefficient in the nonlinear regime, although it leads to the increase of the amplitude of the radial velocity ($V_1 = V_0 \sqrt{k_0^2 + 3}$).

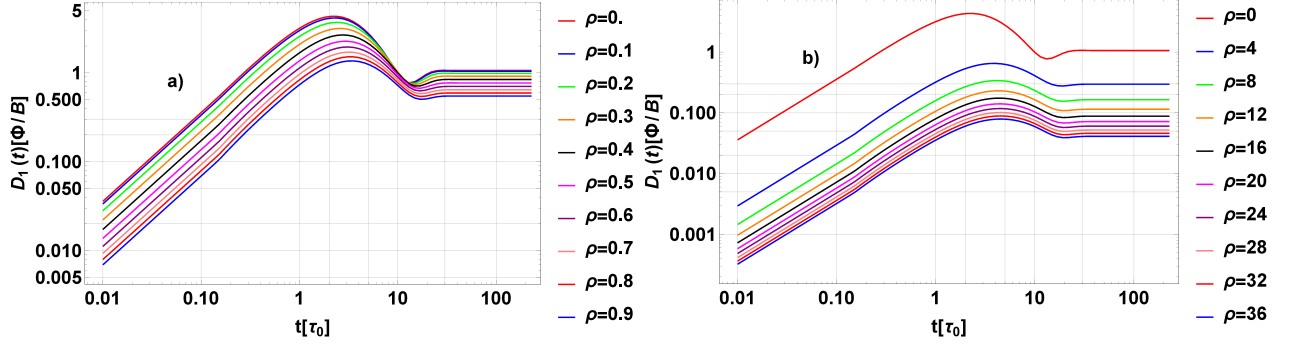


FIG. 6: a) The time dependent diffusion coefficient $D_1(t)$ for $\bar{\rho} \in [0, 1]$ and b) for $\bar{\rho} \in [0, 18]$ with $K_d = 10$ and $V_d = 0.1$

Thus, at large Larmor radius, the time dependent diffusion coefficients are qualitatively similar to those for $\bar{\rho} = 0$. This is also suggested by the shape of the gyro-averaged EC (9), which is not much changed compared to that for $\bar{\rho} = 0$.

B. Fast particle transport regimes

The dependence of the diffusion coefficient $D_1(t)$ on $\bar{\rho}$ is shown in Figure 6. The shapes of the curves are roughly similar for different values of $\bar{\rho}$. The differences between the curves with different $\bar{\rho}$ are practically independent on time, except for the range $\bar{\rho} < 1$ where a stronger dependence on time can be seen (Figure 6a).

The asymptotic diffusion coefficients D_i^∞ are represented in Figure 7 in the nonlinear regime. Figure 7a shows the dependence on the Larmor radius $\bar{\rho}$. One can see that both D_1^∞ and D_2^∞ do not depend on $\bar{\rho}$ for $\bar{\rho} \ll 1$, and that they decay at large $\bar{\rho}$ as $1/\bar{\rho}$. This decay is the same as in the quasilinear regime. Fast particle diffusion coefficient can be evaluated analytically in the case of the quasilinear (Gaussian) transport. It decreases as $1/\bar{\rho}$. The similar dependence on $\bar{\rho}$ in the nonlinear and quasilinear regimes is rather surprising because several works have found a weaker decay in the nonlinear regime (as $1/\bar{\rho}^{0.38}$ in [21]).

The cause of the faster decay with $\bar{\rho}$ found here is the special shape (2) of the spectrum of the drift type turbulence. The average over the gyro motion leads to the attenuation of the large k components of the spectrum ($k\bar{\rho} \gtrsim 1$), while the small k ($k\bar{\rho} \ll 1$) part of S is not affected. The spectrum (2) decays in the small k range because the modes are stable for $k_2 = 0$. Due to this property, all the components of the spectrum are attenuated at large enough values of $\bar{\rho}$ because the condition $k\bar{\rho} \gtrsim 1$ applies for all components that correspond to significant (not close to zero) values of S . This leads at large values of $\bar{\rho}$ to the change of the effective EC that consists only in the decay of the amplitude but not in the modification of the shape (increase of the correlation lengths like for monotonically decaying spectra).

From Figure 7b one can see that the asymptotical value of the diffusion coefficients D_i^∞ does not depend on the value of the k_0 wave vector for $k_0 < 1$ and that it has a weak exponential decay at large k_0 .

The dependence of D_i^∞ of the fast ions on the decorrelation parameter K_d is shown in Figure 7c. One can see that the diffusion coefficients are smaller than in the zero Larmor radius limit (dashed curves). The dependence on K_d of the fast particle diffusion coefficient is the same as at $\rho = 0$ for both limits of small and large K_d (the curves are parallel in these limits). The maximum of $D_1^\infty(K_d)$ is displaced to larger values of K_d at large $\bar{\rho}$. In Figure 7d is plotted the dependence of D_i^∞ on the normalized effective diamagnetic velocity V_d . The behaviour is similar as in the case of vanishing Larmor radius (dashed lines) both in the nonlinear and in the quasilinear regimes.

C. Alpha particle turbulent loss as function of the energy

Numerical simulations have shown that the main decorrelation mechanism in ITG turbulence is the parallel ion motion. The turbulent transport of the fast particles, which have much smaller parallel time τ_z , is completely dominated by the parallel decorrelation. The decorrelation parameter (16) becomes $K_d \cong \tau_z$ in these conditions.

Both the decorrelation time and the Larmor radius are functions of the energy of the α particles. The cooling of the fast particles determine the decrease of $\bar{\rho}$ and the increase of τ_z , but the product of these parameters $\bar{\rho}\tau_z = (m_\alpha/q_\alpha)(\lambda_z/B)$ does not depend on α particle energy. It essentially depends on plasma size through λ_z . In terms of

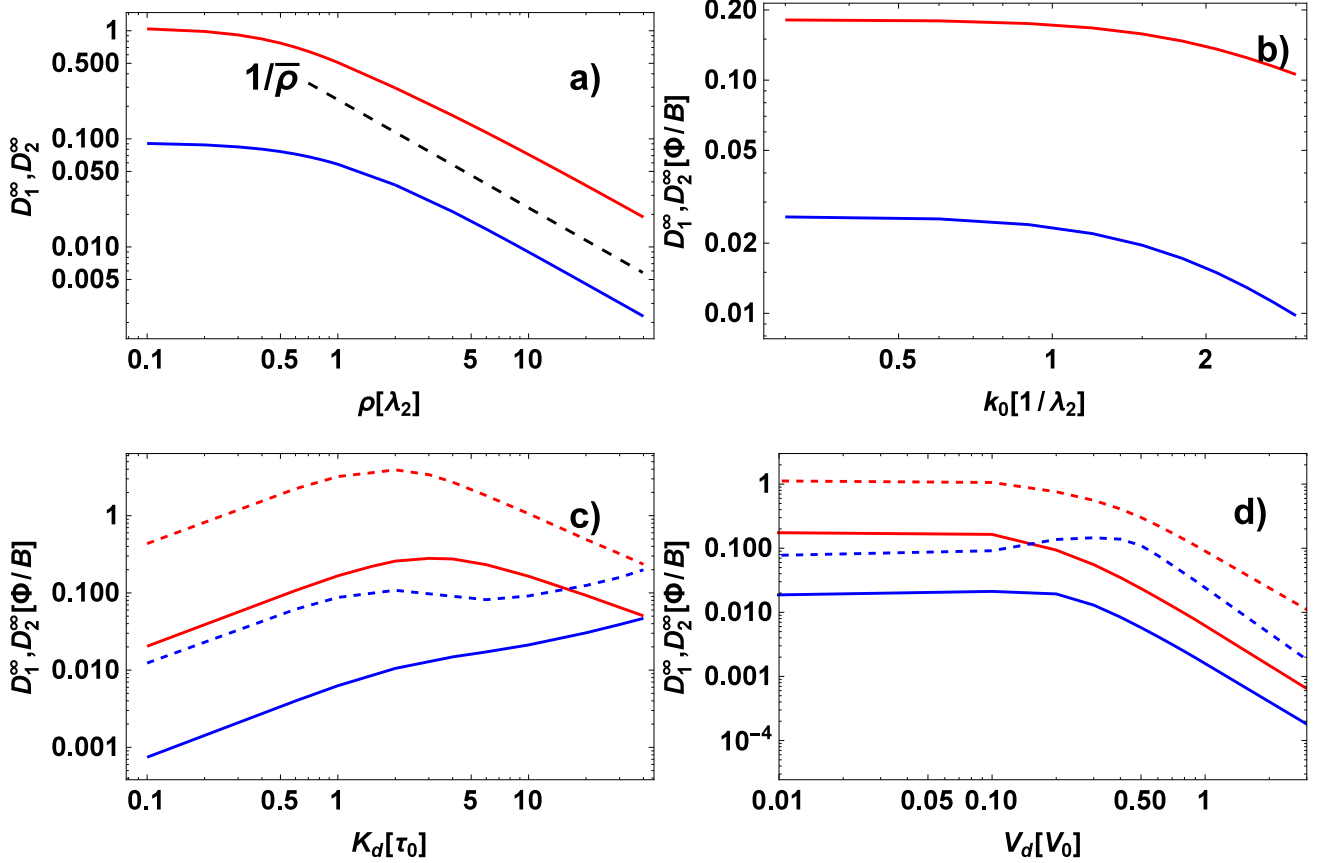


FIG. 7: The asymptotic diffusion coefficients D_1^∞ (red line) and D_2^∞ (blue line). The dashed colored lines correspond to $\bar{\rho} = 0$. The constant parameters are $\bar{\rho} = 4, k_0 = 1, a = 9, K_d = 10$ and $V_d = 0.1$. The dashed line in a) corresponds to the function $1/\bar{\rho}$.

the dimensionless parameters that characterize fast particle transport

$$\bar{\rho}\tau_z = p, \quad p \equiv \mathcal{V} \frac{\lambda_z}{R} \frac{R}{L_{T_i}} \left(\frac{\rho_{ion}}{\lambda_y} \right)^2, \quad \mathcal{V} \equiv \frac{\Phi}{B\lambda_y V_*}, \quad (20)$$

where \mathcal{V} is the ratio of the $\mathbf{E} \times \mathbf{B}$ and diamagnetic velocities. This shows that $\bar{\rho}$ and τ_z (actually K_d) cannot be modified independently for ITG turbulence. Their product is p , a dimensionless parameter that depends on the amplitude of the turbulence (through \mathcal{V}), on its normalized poloidal and parallel correlation lengths and on the gradient length of the ion temperature. Taking the typical parameters of the ITG instabilities for ITER size plasmas similar to those of the present tokamaks (as obtained in numerical simulations), one finds $p \cong 30 (\rho_{ion}/\lambda_y)^2$ (for $R/L_{T_i} \cong 5$, $\lambda_z = 2\pi R$ and $\mathcal{V} \cong 1$).

The dependence of the diffusion coefficient on α particle energy is shown in Figure 8 for several values of p . One can see an important difference between these results and those in Figure 7a, which shows that the decrease of the energy (of $\bar{\rho}$) determines a monotonous increase of the diffusion coefficient. A maximum radial diffusion appears in Figure 8, which has the amplitude and the location dependent on the parameter p . The shape of these curves is determined by the simultaneous variation of $\bar{\rho}$ and τ_z with the energy. The decrease of the energy determines the increase of τ_z , which moves from the small decorrelation time regime in Figure 7c toward the maximum and further to the nonlinear regime with decaying $D_1^\infty(K_d)$. The maxima of the curves in Figure 8 correspond to the maximum of $D_1^\infty(K_d)$ in Figure 7c. This maximum is a decreasing function of the energy, and this is reflected in Figure 8, which shows that the maximum is smaller when it appears at larger energies. The diffusion coefficient in Figure 8 is small for all the range of α particle energy at $p = 40$, but at smaller values of p it can reach significant values (comparable to the ion diffusion coefficient) at energies much larger than plasma ion energy (see the curve for $p = 10$).

Thus, α particle turbulent transport strongly depends on the parameter p , which is determined by the characteristics of the turbulence. Using typical values for the physical quantities in Eq. (20), the main contribution appears to be

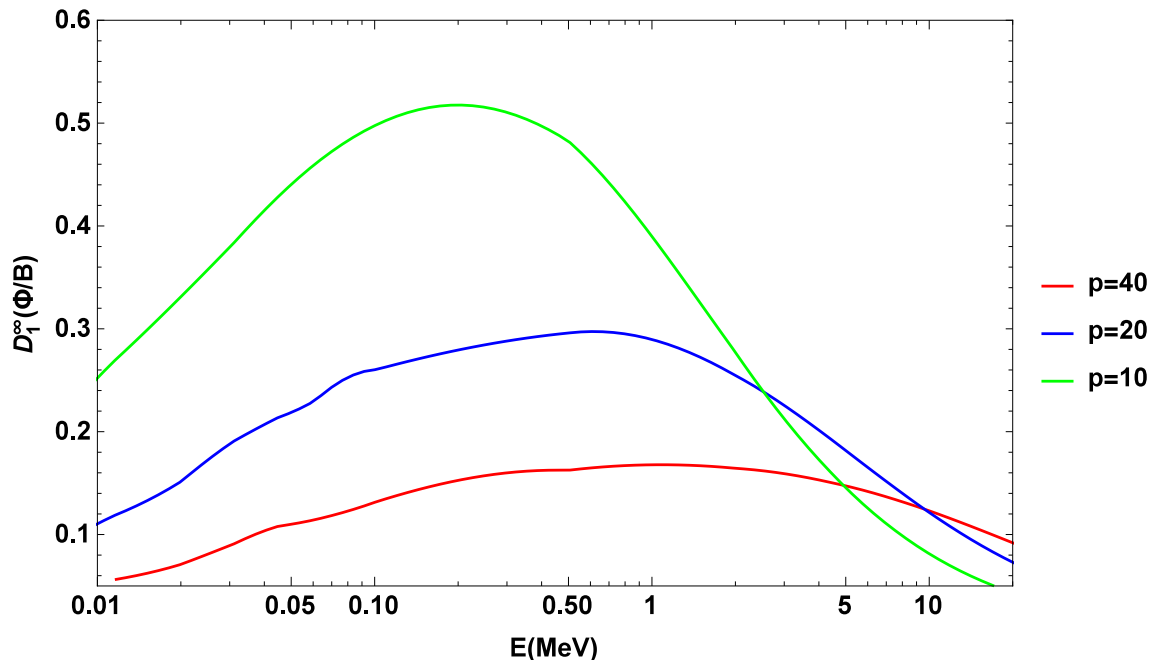


FIG. 8: Asymptotic values of diffusion coefficient D_1^∞ as function of the energy for the values of p that label the curves.

determined by the poloidal correlation length of the turbulence $\bar{\lambda}_y = \lambda_y/\rho_i$. A maximum diffusion coefficient $D_1^\infty \cong 0.5$ appears in Figure 8 for α particle energy of 100KeV if $\bar{\lambda}_y \cong 2$.

IV. CONCLUSIONS

A detailed study of the turbulent transport of the fast α particles was performed based on the development of the DTM. A realistic model of the turbulence was considered. It was necessary to determine numerically the gyro-averaged Eulerian correlation (EC) and to adapt the DTM code to the discretized EC. The code calculates the time dependent diffusion coefficient from the EC and its derivatives represented on a space mesh, using an interpolation procedure.

The dependence of the diffusion coefficient on the five dimensionless parameters of the model ($K_d, V_d, k_0, a, \bar{\rho}$) was determined and analyzed.

The special shape of the spectrum of the ITG turbulence leads to the decay of the diffusion coefficient as $1/\bar{\rho}$ for $\bar{\rho} \gtrsim 2$ for both quasilinear and nonlinear regimes. The decay in the nonlinear regime is faster than in the case of monotonically decreasing Eulerian correlations, as is the one considered in [7]. The difference between the quasilinear and the nonlinear regime is given by a factor that depends on the decorrelation parameter K_d and is smaller at large K_d in the nonlinear regime.

The parallel motion of the α particles provides the main decorrelation mechanism in ITG turbulence. The characteristic time for this motion $\tau_z = \lambda_z/u_z$ depends on α particle energy. It is very small when α particles are born in the nuclear fusion reaction, and it increases by a factor of the order 20 during the cooling process. The dependence of the asymptotic diffusion coefficient on the energy of the α particles was obtained taking into account both the parallel motion and the variation of the Larmor radius. The combined action of these effects leads to the existence of a maximum diffusion coefficient (Figure 8). We have identified a parameter p (20), which includes the characteristics of the turbulence and the plasma size. The maximum turbulent loss rate and the corresponding energy are functions of p . Depending on the specific values of p in a range that is relevant for JET and ITER plasmas, the turbulent transport of the cooling α particles can be negligible or significant. The significant transport appears only when most of the energy of the α particles is lost and their energy is in the range of 100 KeV (see Figure 8).

Acknowledgements

This work was supported by the Romanian Ministry of National Education under the contract 1EU-10 in the Programme of Complementary Research in Fusion. The views presented here do not necessarily represent those of

the European Commission.

-
- [1] S. Zweben, R. Budny, D. Darrow, S. Medley, R. Nazikian, B. Stratton, E. Synakowski, *et al.*, Nuclear Fusion **40**, 91 (2000).
 - [2] S. Zhou, W. Heidbrink, H. Boehmer, R. McWilliams, T. Carter, S. Vincena, and S. Tripathi, Physics of Plasmas (1994-present) **18**, 082104 (2011).
 - [3] S. Zhou, W. Heidbrink, H. Boehmer, R. McWilliams, T. Carter, S. Vincena, S. Tripathi, P. Popovich, B. Friedman, and F. Jenko, Physics of Plasmas (1994-present) **17**, 092103 (2010).
 - [4] J. Dewhurst, B. Hnat, and R. Dendy, Plasma Physics and Controlled Fusion **52**, 025004 (2010).
 - [5] W. Heidbrink, J. M. Park, M. Murakami, C. Petty, C. Holcomb, and M. Van Zeeland, Physical review letters **103**, 175001 (2009).
 - [6] C. Angioni, A. Peeters, G. Pereverzev, A. Bottino, J. Candy, R. Dux, E. Fable, T. Hein, and R. Waltz, Nuclear Fusion **49**, 055013 (2009).
 - [7] T. Hauff and F. Jenko, Physics of Plasmas **13**, 102309 (2006).
 - [8] T. Hauff and F. Jenko, Physics of Plasmas **15**, 112307 (2008).
 - [9] C. Angioni and A. Peeters, Physics of Plasmas (1994-present) **15**, 052307 (2008).
 - [10] J. Chowdhury, W. Wang, S. Ethier, J. Manickam, and R. Ganesh, Physics of Plasmas (1994-present) **19**, 042503 (2012).
 - [11] W. Zhang, V. Decyk, I. Holod, Y. Xiao, Z. Lin, and L. Chen, Physics of Plasmas (1994-present) **17**, 055902 (2010).
 - [12] W. Zhang, Z. Lin, L. Chen, *et al.*, Physical review letters **101**, 095001 (2008).
 - [13] S. Günter, G. Conway, H.-U. Fahrbach, C. Forest, M. G. Muñoz, T. Hauff, J. Hobirk, V. Igochine, F. Jenko, K. Lackner, *et al.*, Nuclear Fusion **47**, 920 (2007).
 - [14] P. W. Gingell, S. C. Chapman, and R. Dendy, Plasma Physics and Controlled Fusion **56**, 035012 (2014).
 - [15] D. Pace, M. Austin, E. Bass, R. Budny, W. Heidbrink, J. Hillesheim, C. Holcomb, M. Gorelenkova, B. Grierson, D. McCune, *et al.*, Physics of Plasmas (1994-present) **20**, 056108 (2013).
 - [16] C. Estrada-Mila, J. Candy, and R. Waltz, Physics of Plasmas (1994-present) **13**, 112303 (2006).
 - [17] M. Vlad, F. Spineanu, S. Itoh, M. Yagi, and K. Itoh, Plasma Physics and Controlled Fusion **47**, 1015 (2005).
 - [18] M. Vlad, F. Spineanu, J. Misguich, and R. Balescu, Physical Review E **58**, 7359 (1998).
 - [19] M. Vlad and F. Spineanu, Physical Review E **70**, 056304 (2004).
 - [20] M. Vlad and F. Spineanu, Physics of Plasmas **22**, 112305 (2015).
 - [21] T. Hauff and F. Jenko, Physics of Plasmas (1994-present) **14**, 092301 (2007).
 - [22] M. W. Shafer, R. Fonck, G. McKee, C. Holland, A. White, and D. Schlossberg, Physics of Plasmas **19** (2012).
 - [23] T. Hahm, W. Lee, and A. Brizard, Physics of Fluids (1958-1988) **31**, 1940 (1988).
 - [24] R. G. Littlejohn, Journal of Mathematical Physics **23**, 742 (1982).
 - [25] M. Vlad and F. Spineanu, Physics of Plasmas **20**, 122304 (2013).